

Epitaxial growth of undoped and Li-doped NiO thin films on α -Al₂O₃ substrates by mist chemical vapor deposition

Takumi Ikenoue*, Junki Inoue, Masao Miyake, and Tetsuji Hirato

Graduate School of Energy Science, Kyoto University, Kyoto 606-8501, Japan

E-mail: ikenoue.takumi.4m@kyoto-u.ac.jp

Abstract

Undoped and Li-doped NiO thin films were grown on α -Al₂O₃ (0001) substrates by mist chemical vapor deposition. Both undoped and Li-doped NiO thin films grew bi-epitaxially on the substrates with crystallographic orientation relationships of NiO(111)[110]|| α -Al₂O₃(0001)[0110] and NiO(111)[110]|| α -Al₂O₃(0001)[0110]. In the Li-doped NiO thin film, a periodic structure was observed, in accordance with a mirror-symmetrical oxygen layer on the terraces of the substrate. Both undoped and Li-doped NiO thin films exhibited high transmittance (>80%) in the visible-light region and optical bandgaps of 3.7–3.8 eV. The undoped NiO thin film showed insulating properties and a resistivity of 10⁶ Ω ·cm or higher. In contrast, the Li-doped NiO thin films had resistivities of 10¹–10⁵ Ω ·cm, depending on the Li precursor concentration. Furthermore, they exhibited positive Seebeck coefficients, indicating their p-type conductivity. These results indicate that Li dopants effectively act as acceptors in NiO thin films.

Keywords

A3.Mist CVD; B2.Wide bandgap oxide semiconductor; B1.Nickel oxide; B1.Li-doped nickel oxide

Highlights

- Epitaxial growth of NiO thin films on α -Al₂O₃ substrate by mist CVD was realized.
- The optical bandgap was calculated as 3.7–3.8 eV.
- Li doping realized p-type conductivity and wide-range conductivity control.

1. Introduction

Wide-bandgap semiconductors, typified by SiC (3.3 eV) and GaN (3.4 eV), attract wide attention because they can produce devices with high output, high breakdown voltage, high frequency, and high heat resistance. Oxide semiconductors such as Ga₂O₃ (4.5–5.0 eV) allow further expansion of the bandgap, and studies on these materials are actively conducted [1,2]. For example, a high-performance Schottky barrier diode using Ga₂O₃ has been realized [3]. The expectation for wide-bandgap oxide semiconductors is increasing, but many wide-bandgap oxide semiconductors, including Ga₂O₃, exhibit only n-type conductivity. In order to realize bipolar devices such as metal oxide semiconductor field-effect transistors, p-type conductivity control is essential. NiO (3.7 eV) has attracted attention for this purpose, as it is a rare wide-bandgap p-type oxide semiconductor. Furthermore, the resistivity of NiO can be controlled by the introduction of Ni vacancies and/or monovalent atoms such as Li by doping [4].

NiO (or Li-doped NiO) has been manufactured by pulsed laser deposition (PLD) [5,6], sputtering [7,8], thermal oxidation of Ni [9], sol-gel methods [10], and so on. In this study, we utilized the mist chemical vapor deposition (CVD) method [2,11–17], which enables high-quality film formation under atmospheric pressure, for the epitaxial growth of NiO thin films on α -Al₂O₃ substrates. Although there are currently no reports of NiO thin films being grown by this method, there is good possibility of it being suitable, as it has been successfully used for the growth of high-quality n-type wide-bandgap oxide semiconductors such as α -Ga₂O₃ [2], β -Ga₂O₃ [14], ϵ -Ga₂O₃ [15], and ZnMgO [16,17]. With regard to device application, it is desirable for NiO thin films to be prepared by the mist CVD method. In addition, we consider electrical conductivity control of the NiO thin film by Li doping.

2. Experiments

Prior to the growth of NiO, the α -Al₂O₃ (0001) substrates were annealed in air at 1050 °C for 4 h to obtain an atomically flat surface, and then washed in acetone, methanol, and deionized water sequentially in an ultrasonic cleaner. Undoped and Li-doped NiO thin films were grown by the mist CVD method, described elsewhere in detail [2,16,18–20]. The growth conditions of undoped and Li-doped NiO are summarized in Table I. The precursor used for the undoped NiO thin-film growth was nickel acetylacetonate (Ni(acac)₂), which was diluted in deionized water at a concentration of 0.020 mol/L. Ethylenediamine (EDA) was then added, which is an additive for forming complexes with nickel ions. For the Li-doped NiO thin films, the precursor solution was obtained by adding either lithium acetylacetonate (Li(acac)) or lithium hydroxide (LiOH) to the Ni(acac)₂ aqueous precursor solution. The Li concentration was varied from 0 to 2 mmol/L, so that the concentration of Li was 0 to 10 mol.% with respect to Ni. Dry air was used for the carrier and dilution gases, with flow rates of 4.0 and 2.0 L/min respectively.

In order to evaluate the film thickness and crystal structure, X-ray reflectivity (XRR) measurements and X-ray diffraction (XRD) analyses (ω -2 θ scans, ω -scan rocking curves, pole figure measurements, and reciprocal space mapping) were carried out using a Panalytical X'pert PRO MPD system. The surface morphology of the films was observed by atomic force microscopy (AFM) (SII Nano Technology, Nano Navi IIS Nanocute). Transmission electron microscopy (TEM) (JEOL, JEM-2100F) was used for cross-sectional observations and selected area electron diffraction (SAED) pattern observations of thin specimens prepared by focused ion beam (FIB) (JEOL, JIB-4000). UV-Vis spectral analysis was done using a UV-Vis spectrophotometer (Shimadzu, UV-2450). The electrical resistivity of the films was determined by the four-terminal method

using a source measure unit (Keithley, 2450 SourceMeter), taking the film thickness as that obtained from XRR measurements. Vacuum-deposited Au was used as an electrode.

3. Results and discussion

First, the optimum growth temperature was examined. Fig. 1 shows the temperature dependence of the growth rate of the NiO thin film. The growth rate was calculated from the film thickness, obtained by XRR measurements, and the growth time. Initially, the growth rate increased as the temperature increased, until it reached a maximum at 650 °C. At higher growth temperatures, re-evaporation was enhanced, which reduced the growth rate. Moreover, the crystallinity, which was evaluated by the full-width half-maximum (FWHM) of the ω -scan rocking curve for NiO (111) diffraction, was best at 650 °C, and thus this was determined to be the optimum growth temperature. In the subsequent experiments, the growth temperature was set to 650 °C unless otherwise noted.

Fig. 2 shows the XRD pattern from the $2\theta/\theta$ scan of the NiO thin film. Diffraction peaks of NiO (111) and (222) were observed in addition to the diffraction peak of the α -Al₂O₃ (0006) substrate. In the expanded NiO (111) diffraction pattern, clear Laue fringes were observed, suggesting that the NiO thin film was of high quality. The Laue fringes also allowed calculation of the film thickness, which corresponded well with the XRR results. The FWHM of the ω -scan rocking curve for NiO (111) diffraction was as small as 273 arcsec. This value is smaller than that of previously demonstrated NiO thin films on α -Al₂O₃ (0006) substrates, grown by atmospheric pressure metal organic CVD [21], PLD [22], and atomic layer deposition (ALD) [23], suggesting high crystallinity.

The in-plane orientation relationship between NiO and α -Al₂O₃ was established by X-ray pole figure measurements for NiO {002}. The scan results are shown in Fig. 3. Sharp peaks with six-fold rotational symmetry were clearly observed at tilting angles of $\psi = 55^\circ$ and 61° . The pole figure was measured at $2\theta = 43.383^\circ$, which is the diffraction

condition of NiO (002); however, this value is also very close to the condition of α -Al₂O₃ (1123) diffraction ($2\theta = 43.340^\circ$). From the known crystal structure, it is estimated that NiO (002) diffracts at $\psi = 54.7^\circ$ and α -Al₂O₃ (1123) diffracts at $\psi = 61.3^\circ$, so it can be concluded that the obtained peaks are due to these two diffractions. Therefore, in this pole figure, six NiO (002) peaks appeared at the same ϕ angle as the α -Al₂O₃ (113) peaks. This result indicates the presence of twins with a rotation of 180° on the α -Al₂O₃ (0006) surface. On the basis of these XRD measurements and as previously discussed [24], the epitaxial relationships between NiO and α -Al₂O₃ can be written as NiO(111)[$\bar{1}$ 10]|| α -Al₂O₃(0001)[0110] and NiO(111)[110]|| α -Al₂O₃(0001)[0110]. Fig. 4 shows the reciprocal space map (RSM) for the NiO (113) and α -Al₂O₃ (1129) reflections. From the theoretical position of the bulk NiO reflection peak (marked as x), it is considered that the NiO film is subjected to slight in-plane tensile strain and vertical compressive strain under the influence of the α -Al₂O₃ substrate. The in-plane lattice mismatch between NiO and α -Al₂O₃ is 7.5%, considering domain matching epitaxy (DME) [24]. A film in which the lattice constant of the substrate is less than that of the epitaxial layer is generally subjected to in-plane compressive strain and vertical tensile strain. However, the obtained NiO film was subjected to the opposite strain. This may be attributed to the difference in thermal expansion coefficient between α -Al₂O₃ and NiO. At the growth temperature of 650 °C, NiO grows in alignment with the substrate by higher-order common multiple matching and is hardly subjected to strain. Since the NiO film has a larger thermal expansion coefficient ($14 \times 10^{-6} \text{ K}^{-1}$) than the α -Al₂O₃ substrate ($7 \times 10^{-6} \text{ K}^{-1}$), it can be considered that it undergoes in-plane tensile strain on cooling to room temperature. The change of lattice constant (4.4%) estimated from the thermal expansion coefficients and the temperature change very closely agrees with the result of

RSM.

The surface morphology of the undoped NiO thin film was investigated using AFM. The typical AFM image in Fig. 5 shows triangular-shaped domains on a flat surface. The lateral sizes of the domains were in the range of 100–300 nm. It is conceivable that each domain had the same crystal orientation as above, with regard to the orientation of the triangle. Hence, the growth mode of the undoped NiO thin film is supposed to be the Volmer–Weber mode, where nucleation occurs at localized areas.

The obtained NiO thin films showed insulating properties and a resistivity of 10^6 $\Omega\cdot\text{cm}$ or higher. Thus, we doped them with Li to improve their electrical characteristics. Li(acac) and LiOH were investigated as potential dopants. Fig. 6 shows the XRD patterns from $2\theta/\theta$ scans of Li-doped NiO thin films obtained with different Li precursors and concentrations. Similarly to the undoped thin film, only NiO (111) and NiO (222) diffraction peaks were observed. In addition, the same peak profiles were observed from the pole figure measurement. Thus, it was confirmed that the in-plane orientation relationship was the same as that of undoped NiO.

Interestingly, the thin film with the flattest surface was obtained from a precursor solution of 1% Li(acac), where the root mean square surface roughness was 1.21 nm. As shown in the AFM image in Fig. 7, this Li-doped NiO thin film had a periodic structure with a width of about 70 nm. This width coincides with the terrace width of the $\alpha\text{-Al}_2\text{O}_3$ substrate, suggesting that the Li-doped NiO thin film grows on each terrace of the $\alpha\text{-Al}_2\text{O}_3$ substrate, with grain boundaries at the step positions. This periodic structure has been reported previously with regard to NiO thin films on sapphire substrates [25], where two types of mirror-symmetrical terraces exist in accordance with the step height. It was found that “NiO [grew epitaxially] on the 0.22-nm-high-stepped sapphire (0001) plane to match

the mirror-symmetrical oxygen layer between the adjacent substrate terraces.” [25] It is conceivable that the periodic structure of the Li-doped NiO thin film obtained by the mist CVD method has the same structure. Therefore, observations were conducted using TEM to confirm whether the periodic structure was of bi-epitaxially grown NiO according to the two types of terraces of the α -Al₂O₃ substrate. Fig. 8 (a) shows a cross-sectional TEM image and Fig. 8 (b) shows a high-resolution (HR) TEM image of the Li-doped NiO thin film. A lattice spacing of 0.24 nm, which can be readily indexed to the (111) crystal plane of NiO, was observed from Fig. 8 (b), and epitaxial growth of the Li-doped NiO thin films along the (111) orientation was confirmed. Figs. 8 (c) and (d) are SAED patterns obtained from the respective regions shown in Fig. 8 (e). These SAED patterns were observed alternately and periodically. From these SAED images, it can be confirmed that single-crystal NiO grew according to the terraced surface of the α -Al₂O₃ substrate, and bi-epitaxial growth occurred. From these results and AFM images (Fig. 7), it is suggested that this Li-doped NiO thin film was epitaxially grown on each terrace of the stepped α -Al₂O₃ (0001) substrate, and has a structure as shown in Fig. 9 which was drawn using Vesta software [26].

To assess the potential of the NiO thin films, the optical and electrical properties were described. Fig. 10 shows the transmittance spectra and Tauc plot of the undoped and Li-doped NiO thin films. In the transmittance spectra, a marked decrease in the transmission rate occurred at wavelengths shorter than 330 nm, which is clearly due to absorption by NiO. The bandgaps calculated from the Tauc plot $[(\alpha hv)^2 - hv]$ were almost constant irrespective of Li doping (3.7–3.8 eV). The electrical resistivity of the Li-doped NiO thin film obtained from each Li precursor solution is shown in Fig. 11. The obtained undoped NiO thin film showed insulating properties and a resistivity of $10^6 \Omega \cdot \text{cm}$ or

higher. In contrast, the resistivity of the Li-doped NiO thin film was 1 to 5 orders of magnitude smaller (10^1 – $10^5 \Omega\cdot\text{cm}$). All the Li-doped NiO thin films exhibited positive Seebeck coefficients, indicating their p-type conductivity. These results indicated that the Li dopant acts as an acceptor, increasing the carrier concentration.

4. Conclusions

NiO thin films were epitaxially grown on α -Al₂O₃ substrates by mist CVD. Undoped and Li-doped NiO thin films grew bi-epitaxially on the substrates with crystallographic orientation relationships of NiO(111)[$\bar{1}$ 10] \parallel α -Al₂O₃(0001)[0110] and NiO(111)[110] \parallel α -Al₂O₃(0001)[0110]. The optical bandgap calculated by the Tauc plot obtained from the transmittance spectra was 3.7–3.8 eV. The electrical resistivity of the NiO thin film, which was higher than 10⁶ Ω ·cm in the undoped sample, was improved to 10¹–10⁵ Ω ·cm by Li doping. The positive Seebeck coefficient shows the p-type conductivity of the Li-doped NiO thin films, indicating that Li can be doped effectively into NiO thin films.

Acknowledgments

Part of this study was supported by NIMS Nanofabrication Platform under the Nanotechnology Platform Project sponsored by the Ministry of Education, Culture, Sports, Science and Technology (MEXT), Japan. This work also was supported by JSPS Early-Career Scientists (JP18K13788).

References

- [1] T. Oshima, T. Okuno, N. Arai, N. Suzuki, H. Hino, S. Fujita, *Jpn. J. Appl. Phys.* 48 (2009) 011605.
- [2] D. Shinohara, S. Fujita, *Jpn. J. Appl. Phys.* 47 (2008) 7311–7313.
- [3] M. Oda, R. Tokuda, H. Kambara, T. Tanikawa, T. Sasaki, T. Hitora, *Appl. Phys. Express* 9 (2016) 021101.
- [4] T. Kamiya, H. Ohta, M. Kamiya, K. Nomura, K. Ueda, M. Hirano, H. Hosono, *J. Mater. Res.* 19 (2004) 913–920.
- [5] R. Molaie, R. Bayati, J. Narayan, *Cryst. Growth Des.* 13 (2013) 5459–5465.
- [6] J.Y. Zhang, W.W. Li, R.L.Z. Hoye, J.L. MacManus-Driscoll, M. Budde, O. Bierwagen, L. Wang, Y. Du, M.J. Wahila, L.F.J. Piper, T.-L. Lee, H.J. Edwards, V.R. Dhanak, K.H.L. Zhang, *J. Mater. Chem. C* 6 (2018) 2275–2282.
- [7] H. Sato, T. Minami, S. Takata, T. Yamada, *Thin Solid Films* 236 (1993) 27–31.
- [8] M. Sugiyama, H. Nakai, G. Sugimoto, A. Yamada, S.F. Chichibu, *Jpn. J. Appl. Phys.* 55 (2016) 088003.
- [9] Z. Zhang, Y. Zhao, M. Zhu, *Appl. Phys. Lett.* 88 (2006) 033101.
- [10] Y. Kokubun, Y. Amano, Y. Meguro, S. Nakagomi, *Thin Solid Films* 601 (2016) 76–79.
- [11] H. Nishinaka, T. Kawaharamura, S. Fujita, *Jpn. J. Appl. Phys.* 46 (2007) 6811–6813.
- [12] T. Kawaharamura, H. Nishinaka, S. Fujita, *Jpn. J. Appl. Phys.* 47 (2008) 4669–4675.
- [13] T. Ikenoue, S. Sakamoto, Y. Inui, *Jpn. J. Appl. Phys.* 53 (2014) 05FF06.
- [14] S. Lee, K. Kaneko, S. Fujita, *Jpn. J. Appl. Phys.* 55 (2016) 1202B8.
- [15] H. Nishinaka, D. Tahara, M. Yoshimoto, *Jpn. J. Appl. Phys.* 55 (2016) 1202BC.
- [16] H. Nishinaka, Y. Kamada, N. Kameyama, S. Fujita, *Phys. Status Solidi* 247 (2010) 1460–1463.
- [17] K. Kaneko, T. Onuma, K. Tsumura, T. Uchida, R. Jinno, T. Yamaguchi, T. Honda, S. Fujita, *Appl. Phys. Express* 9 (2016) 111102.
- [18] H. Nishinaka, Y. Kamada, N. Kameyama, S. Fujita, *Jpn. J. Appl. Phys.* 48 (2009) 121103.
- [19] K. Akaiwa, S. Fujita, *Jpn. J. Appl. Phys.* 51 (2012) 070203.
- [20] N. Suzuki, K. Kaneko, S. Fujita, *J. Cryst. Growth* 364 (2013) 30–33.
- [21] T.M. Roffi, S. Nozaki, K. Uchida, *J. Cryst. Growth* 451 (2016) 57–64.
- [22] Y. Kakehi, S. Nakao, K. Satoh, T. Kusaka, *J. Cryst. Growth* 237–239 (2002) 591–595.
- [23] E. Lindahl, J. Lu, M. Ottosson, J.-O. Carlsson, *J. Cryst. Growth* 311 (2009) 4082–4088.
- [24] J.H. Lee, Y.H. Kwon, B.H. Kong, J.Y. Lee, H.K. Cho, *Cryst. Growth Des.* 12 (2012)

2495–2500.

- [25] R. Yamauchi, Y. Hamasaki, T. Shibuya, A. Saito, N. Tsuchimine, K. Koyama, A. Matsuda, M. Yoshimoto, *Sci. Rep.* 5 (2015) 14385.
- [26] K. Momma, F. Izumi, *J. Appl. Crystallogr.* 44 (2011) 1272–1276.

Figure captions

Fig. 1 Temperature dependence of the growth rate of NiO thin film grown by mist CVD method.

Fig. 2 XRD pattern from the $2\theta/\theta$ scan of the NiO thin film grown at 650 °C. The inset is an expanded view of the NiO (111) diffraction peak.

Fig. 3 XRD pole figure for {002} planes of the NiO thin film measured at $2\theta = 43.383^\circ$. Diffraction of $\alpha\text{-Al}_2\text{O}_3$ {1123} plane ($2\theta = 43.340^\circ$) is also observed in this pole figure.

Fig. 4 XRD reciprocal space map for NiO (113) and $\alpha\text{-Al}_2\text{O}_3$ (1129) reflection. **X** represents the theoretical position of bulk NiO reflection peaks.

Fig. 5 AFM image of undoped NiO thin film grown at 650 °C.

Fig. 6 XRD patterns from $2\theta/\theta$ scans of Li-doped NiO thin films obtained with each Li precursor and Li concentration.

Fig. 7 AFM image of the Li-doped NiO thin film obtained from Li(acac) 1% source solution.

Fig. 8 (a) TEM and (b) HRTEM images of the Li-doped NiO thin film. (c), (d) SAED images obtained from the respective regions in (e) TEM image.

Fig. 9 Schematic atomic structure for Li-doped NiO thin film grown on an atomically stepped $\alpha\text{-Al}_2\text{O}_3$ substrate. NiO and twined-NiO were epitaxially grown on each terrace of stepped $\alpha\text{-Al}_2\text{O}_3$ substrate.

Fig. 10 Transmittance spectra and Tauc plot of the undoped and Li-doped NiO thin films.

Fig. 11 Electrical resistivity of Li-doped NiO thin films obtained from precursor solutions with different concentrations of Li.

Table I. Growth condition of NiO thin films.

Source, concentration	Ni(acac) ₂ , 0.020 mol/L
Complexing agent, concentration	EDA, 0.040 mol/L
Dopant, concentration	Li(acac) or LiOH, 0–0.002 mol/L
Solvent	Deionized water
Carrier gas, flow rate	Dry air, 4 L/min
Dilution gas, flow rate	Dry air, 2 L/min
Growth temperature	500–750 °C
Growth time	10 min
Substrate, size	$\alpha\text{-Al}_2\text{O}_3$, 10 mm × 10 mm

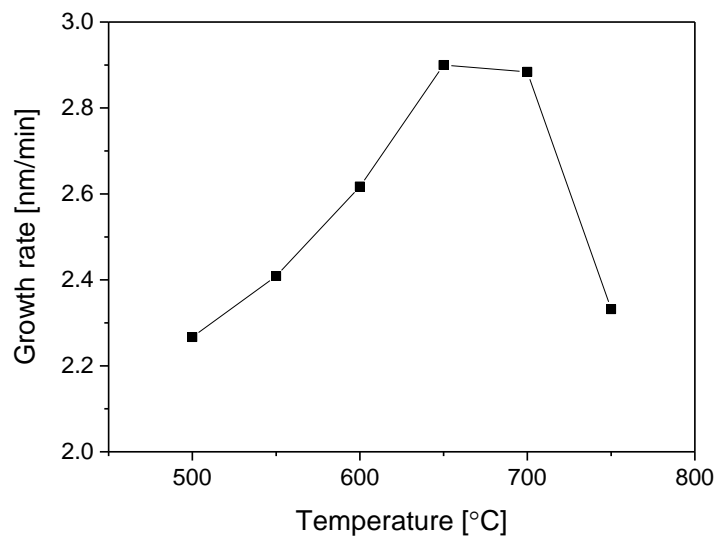


Fig. 1 Temperature dependence of the growth rate of NiO thin film grown by mist CVD method.

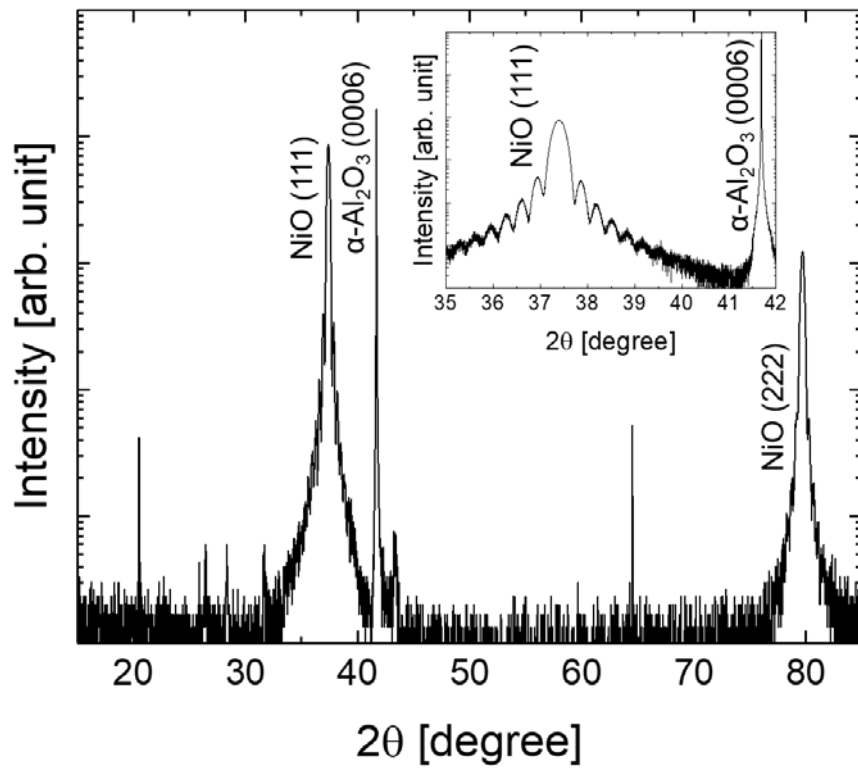


Fig. 2 XRD pattern from the $2\theta/\theta$ scan of the NiO thin film grown at 650 °C. The inset is an expanded view of the NiO (111) diffraction peak.

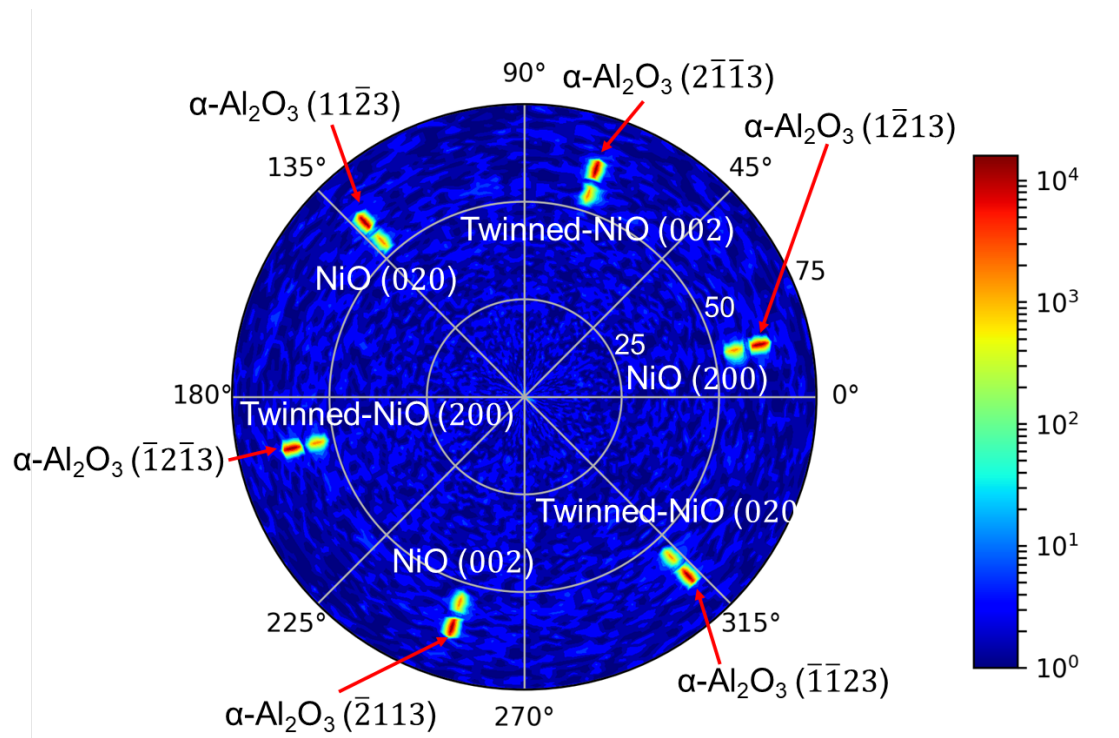


Fig. 3 XRD pole figure for {002} planes of the NiO thin film measured at $2\theta = 43.383^\circ$. Diffraction of $\alpha\text{-Al}_2\text{O}_3$ {1123} plane ($2\theta = 43.340^\circ$) is also observed in this pole figure.

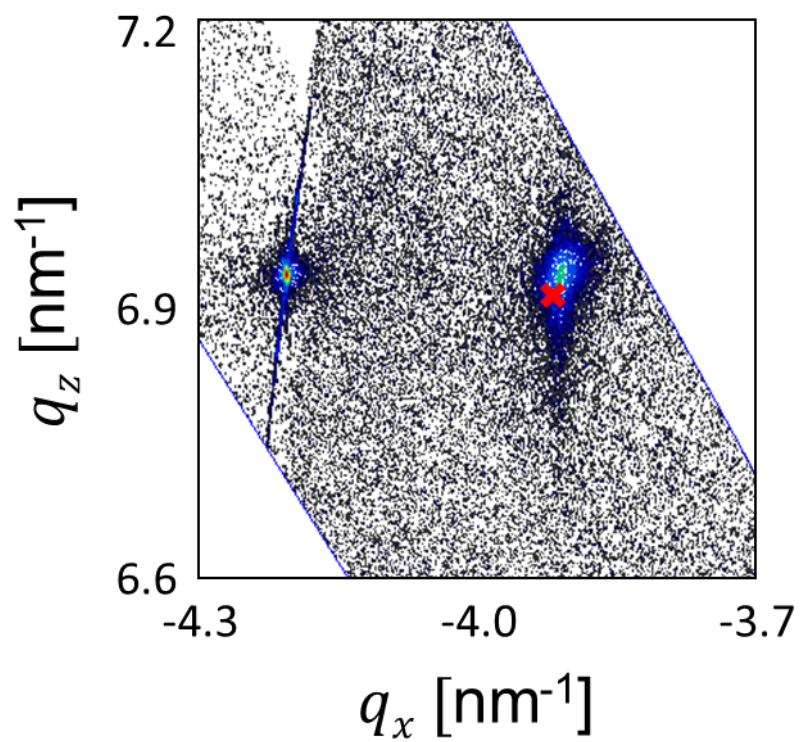


Fig. 4 XRD reciprocal space map for NiO (113) and α -Al₂O₃ (1129) reflection. **x** represents the theoretical position of bulk NiO reflection peaks.

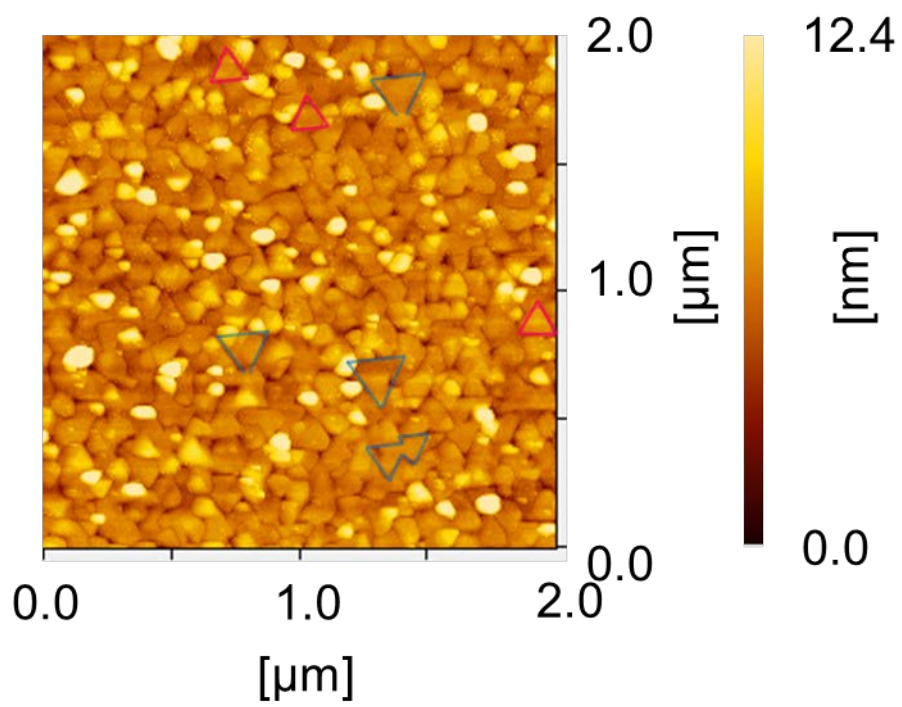


Fig. 5 AFM image of undoped NiO thin film grown at 650 °C.

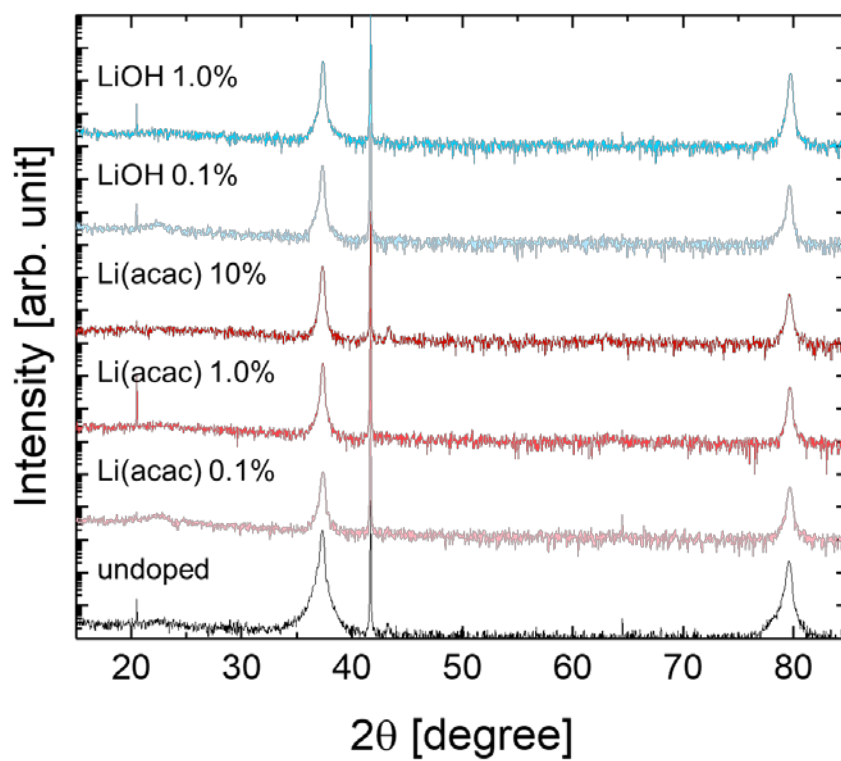


Fig. 6 XRD patterns from $2\theta/\theta$ scans of Li-doped NiO thin films obtained with each Li precursor and Li concentration.

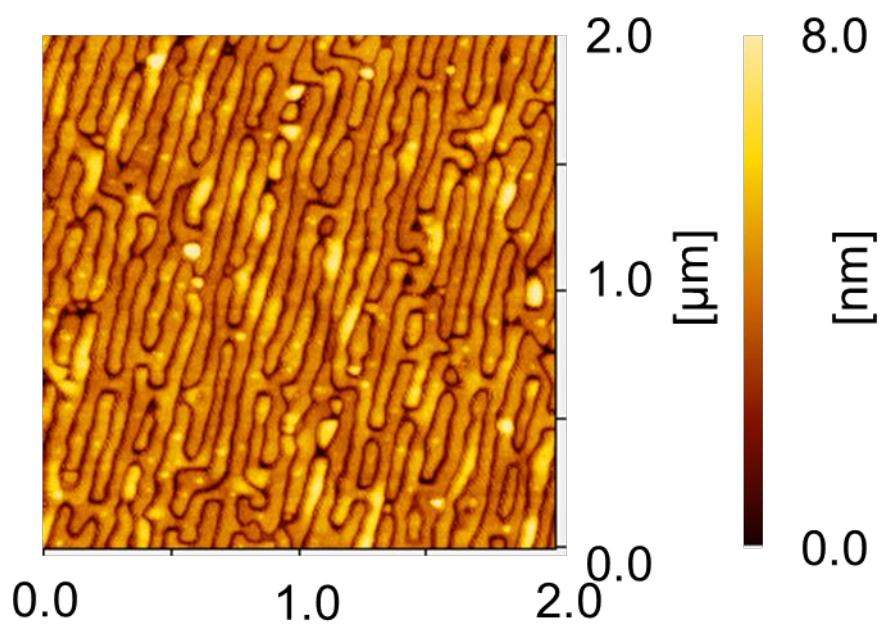


Fig. 7 AFM image of the Li-doped NiO thin film obtained from Li(acac) 1% source solution.

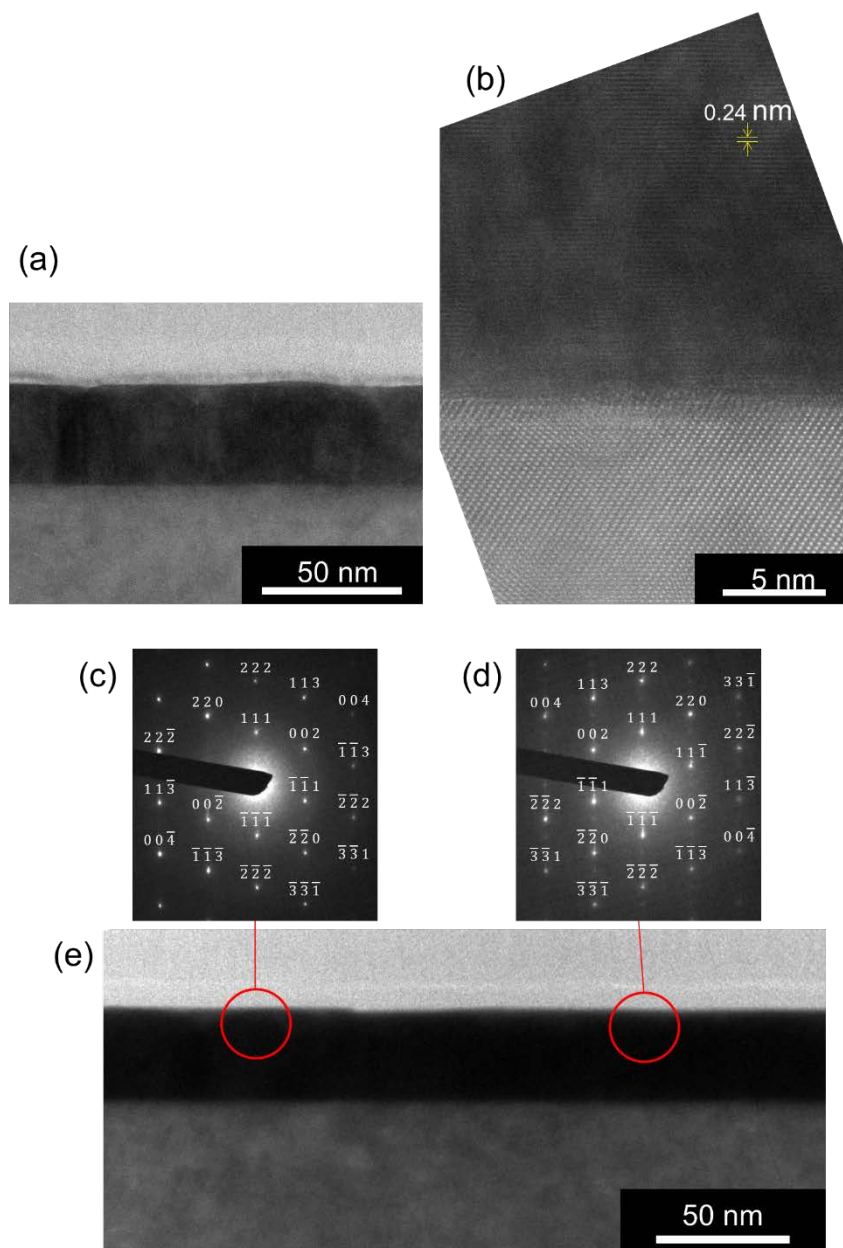


Fig. 8 (a) TEM and (b) HRTEM images of the Li-doped NiO thin film. (c), (d) SAED images obtained from the respective regions in the TEM image in (e).

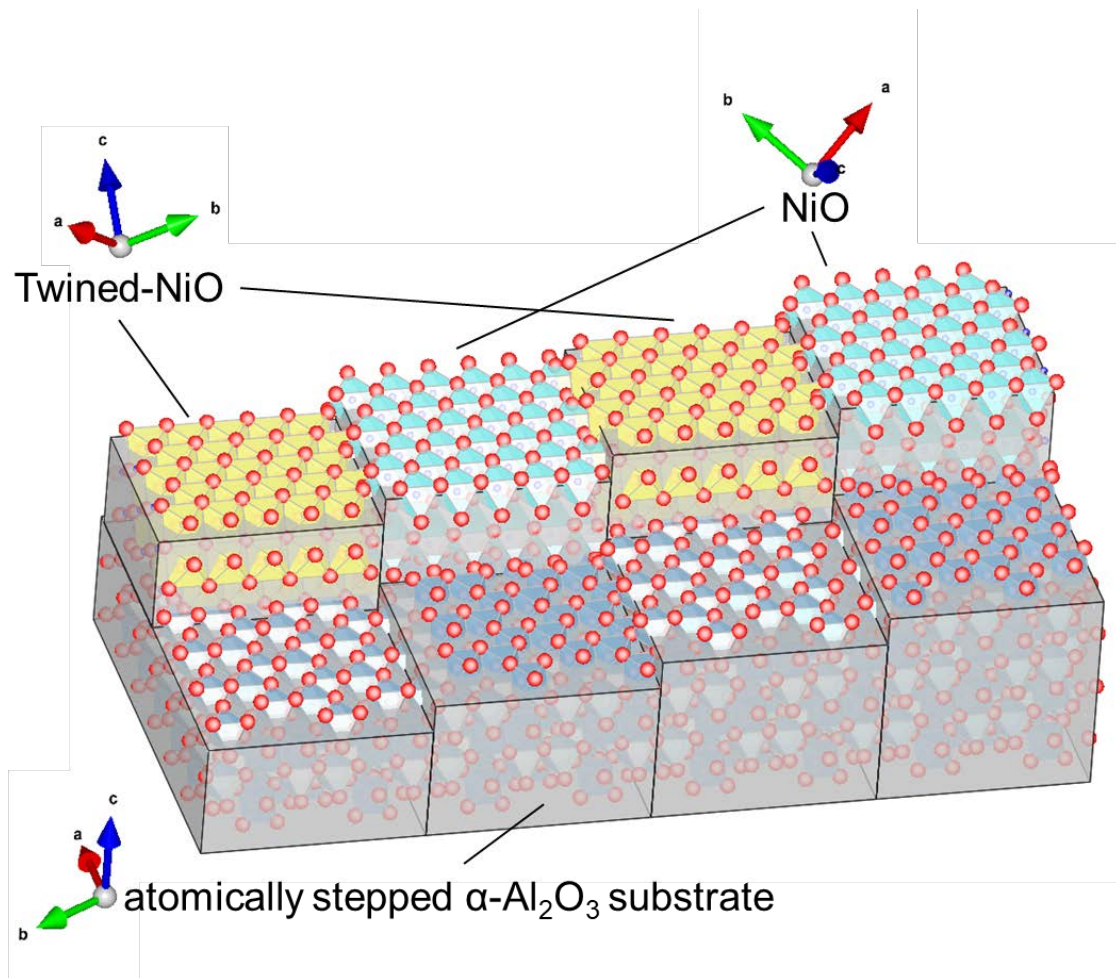


Fig. 9 Schematic atomic structure for Li-doped NiO thin film grown on an atomically stepped α - Al_2O_3 substrate. NiO and twined-NiO were epitaxially grown on each terrace of the stepped α - Al_2O_3 substrate.

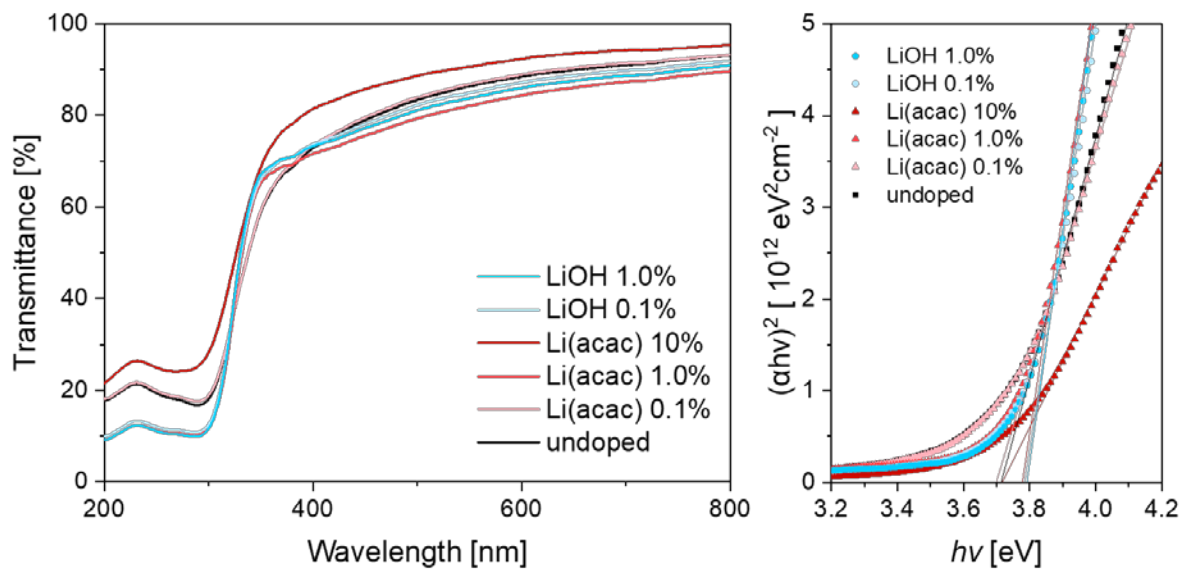


Fig. 10 Transmittance spectra and Tauc plot of the undoped and Li-doped NiO thin films.

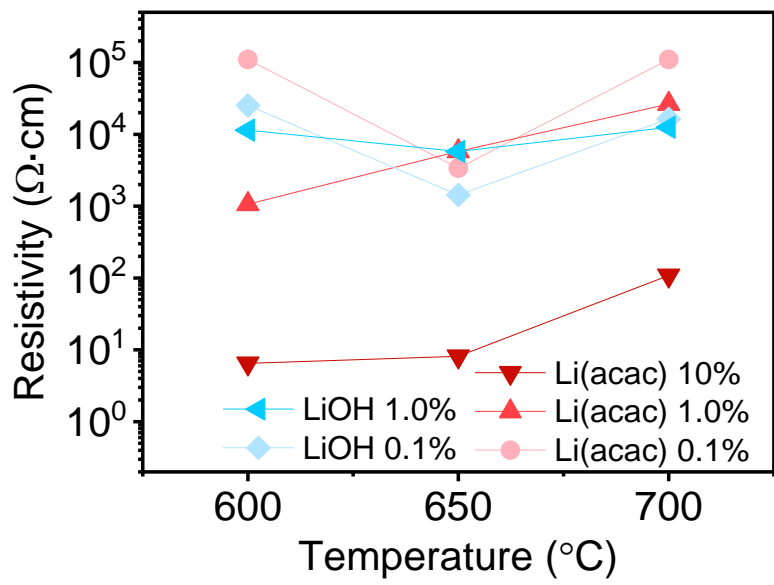


Fig. 11 Electrical resistivity of Li-doped NiO thin films obtained from precursor solutions with different concentrations of Li.